Progress in Oceanography 168 (2018) 296–309

Contents lists available at ScienceDirect

Progress in Oceanography

journal homepage: www.elsevier.com/locate/pocean

Changes across 66°W, the Caribbean Sea and the Western boundaries of the North Atlantic Subtropical Gyre

M. Casanova-Masjoan[a,b], T.M. Joyce[b], M.D. Pérez-Hernández[b,c], P. Vélez-Belchí[d], A. Hernández-Guerra[a,*]

[a] Instituto de Oceanografía y Cambio Global, IOCAG, Universidad de Las Palmas de Gran Canaria, ULPGC, Spain
[b] Department of Physical Oceanography, Woods Hole Oceanographic Institution, Woods Hole, MA, USA
[c] Division Environment, Marine and Freshwater Research Institute, Reykjavik, Iceland
[d] Centro Oceanográfico de Canarias, Instituto Español de Oceanografía, Santa Cruz de Tenerife, Canary Islands, Spain

ARTICLE INFO

Keywords:
Western boundary current
Inverse box model
Geostrophic transport
Western subtropical Atlantic

ABSTRACT

A World Ocean Circulation Experiment Hydrographic Program along with a Global Repeat Hydrography Program occupied sections along 66°W in the North West Atlantic Ocean in 2003 and 2012. Hydrographic variables, tracers and LADCP measurements were collected in situ. This section together with the North American and South American Coasts create a closed volume, excluding any flow through the Panama Canal. Combining mass, silica and LADCP information with constraints in an inverse box model we obtain a strong eastward flow of the Gulf Stream (100.1 ± 4.6 Sv in 2003 and 123.8 ± 4.4 Sv in 2012), and westward flows of the Caribbean Current (−24.4 ± 1.0 Sv in 2003 and −24.2 ± 1.1 Sv in 2012) and Deep Western Boundary Current (DWBC). The DWBC carries the ventilated waters of the Labrador Sea and the Nordic Seas. Comparing the results of 2003 and 2012, an insignificant reduction is observed in the DWBC transport (−17.3 ± 2.9 Sv and −15.0 ± 2.5 Sv for 2003 and 2012, respectively). The net heat fluxes do not show major changes through the section during both cruises (−0.23 ± 0.08 PW in 2003 and −0.21 ± 0.12 PW in 2012). In contrast, freshwater fluxes present positive values in the dry season (0.24 Sv in spring 2012) and negative values in the wet season (−0.32 Sv in fall 2003). The difference between both cruises may be due to seasonal variability in the area.

1. Introduction

The Atlantic Meridional Overturning Circulation (AMOC) refers to the circulation of the superficial warm ocean currents flowing poleward in the Gulf Stream (GS) and the deeper cold waters flowing towards the equator from the Labrador and Nordic Seas in the Deep Western Boundary Current (DWBC) (Stommel, 1965). Both of these current systems are in part compensated by local recirculation and interior flows. In the southern part of the Western North Atlantic Subtropical Gyre there is an island chain from the Bahamas to the northern coast of South America that encloses the deep Caribbean Sea. The water exchange between the Atlantic Ocean and the deep Caribbean Sea takes place through the Antilles passages, most importantly through the Anegada Passage in the lesser Antilles. This is the deepest passage and permits ventilation of the deep Caribbean Sea (Johns et al., 2002). The Caribbean Sea is also a pathway for the recirculation of the North Atlantic Subtropical Gyre and the South Atlantic Waters that are carried northward through the Gulf Stream System (Schmitz and McCartney, 1993; Schmitz and Richardson, 1991).

The A22 is a hydrographic section that crosses the North Atlantic Subtropical Gyre and the Caribbean Sea along 66°W. The first time this section was surveyed was in 1997 during a World Ocean Circulation Experiment (WOCE) Hydrographic Program (WHP) cruise. WOCE is a program that estimated the global ocean circulation state during the 1990's decade (Ganachaud and Wunsch, 2000). However, considering that ocean properties and transports vary over time, the international Global Ocean Ship-bases Investigation Program (GO-SHIP) was created to repeat the hydrographic cruises over the most important WOCE legs once every 10 years (Talley et al., 2016). The importance of the A22 lies in that it crosses the Caribbean current, an extension of the North Equatorial Current (NECC) and North Brazil Current (NBC) (Fratantoni, 2001) which transports ~30 Sv to the west flowing through the Yucatan and Florida Straits to the GS (Gordon, 1967). Furthermore, the Gulf Stream crosses through the northern part of the section once, transporting more than 100 Sv (Joyce et al., 2001), and, finally, the DWBC crosses the section twice, transporting between 18 and 47 Sv

* Corresponding author.
E-mail address: alonso.hernandez@ulpgc.es (A. Hernández-Guerra).

https://doi.org/10.1016/j.pocean.2018.09.013
Received 12 February 2018; Received in revised form 12 September 2018; Accepted 13 September 2018
Available online 14 September 2018
0079-6611/ © 2018 Elsevier Ltd. All rights reserved.

(Hernández-Guerra et al., 2014; Joyce et al., 2001) first to the north of the GS flowing westwards and secondly to the north of Puerto Rico flowing eastwards. The relevance of these prominent ocean currents has led to the repetition of the A22 in both 2003 and 2012.

Our effort in this paper is to compare the absolute geostrophic transports estimated from hydrographic data, Lowered Acoustic Doppler Current Profiler (LADCP), nutrient data and the results of an inverse box model from two cruises carried out in 2003 and 2012 over 66°W in the North Atlantic. Thus, the paper is organized as follow: Section 2 introduces the data from the 2003 and 2012 hydrographic sections; Section 3 presents the methods and results for the initial geostrophic transports for these year; Section 4 explains the details of the inverse box model used to estimate reference velocities and adjusted geostrophic transports; Section 5 explores the estimated adjusted geostrophic transports for the 2003 and 2012 cruises; Section 6 shows the heat and freshwater fluxes through 66°W. We close with a discussion of the main results and the changes which occurred in 1997, 2003 and 2012 across 66°W.

2. Data and vertical sections

2.1. Data

Hydrographic data of two cruises were collected along the A22 section at 66°W in fall 2003 (October 23 to November 13) and spring 2012 (March 24 to April 17) as part of the international program GO-SHIP (Talley et al., 2016). The 2003 cruise was carried out northward, from Trinidad to Cape Cod (MA, USA), and the 2012 cruise worked southward from Cape Cod to Aruba (Leeward Antilles) (Fig. 1). Fig. 1 also shows the A22 hydrographic stations location from 1997 which has been discussed in Joyce et al. (2001). The separation between stations varied depending on the location: in steep topography the separation between stations is ~10 km and ~30 km across the Gulf Stream, and otherwise, the separation is typically ~75 km. At each station a Conductivity-Temperature-Depth (CTD) profile was obtained for the entire water column. Rosette water samples were also taken for oxygen and other chemical tracers. An LADCP provides a velocity profile at each station (http://currents.soest.hawaii.edu/clivar/ladcp/). For the 2003 cruise, a downward and upward-looking 300 kHz LADCP was used for stations 1 to 37, and a downward-looking 150 kHz was used for stations 38 to 82. For the 2012 cruise, a downward-looking 150 kHz was used for all the stations. Cruise reports including data processing and sampling data are available online at https://cchdo.ucsd.edu/. Winds from National Centers for Environmental Prediction (NCEP) reanalysis project from the National Oceanic and Atmospheric Administration (NOAA, https://www.esrl.noaa.gov/) are used to estimate the initial Ekman transports (Kalany et al., 1996).

2.2. Hydrographic sections

Though the determination of water masses is mainly based in potential temperature, salinity, neutral density and potential temperature and salinity diagram (Figs. 2–5 and Table 1), tracers (silica and CFC-11 and CFC-12, Figs. 6–8) have also helped in discerning between the old and new water masses. CFCs are anthropogenic substances that entered the ocean through the atmosphere during the 1990s, and are transported equatorward through the DWBC (LeBel et al., 2008; Stramma et al., 2004). Fig. 5 reveals differences between both cruises at the surface layer. This is due to seasonality: while the 2003 cruise took place in fall, the 2012 took place in spring. Therefore, precipitation and river runoff imprint a fresher surface layer in 2003 than in 2012.

The north wall of the Gulf Stream (GS) is commonly defined as the location of the 15 °C isotherm at 200 m depth (Fuglister, 1955; Joyce et al., 2000). Looking at Fig. 2 this occurs at 38°N in 2003 and 38.4°N in 2012. The northernmost side of our sections extends from the North American Coast to the north wall of the GS. This area has the lowest surface salinity values (< 35.5) (Fig. 3) and temperatures in the range of 10°–15 °C (Fig. 2). These characteristics are easily observed for both sections in the θ-S diagram of both years and correspond with Ford Waters (Fig. 5). Ford Water (FW) originates from the continental freshwater and reaches our area as filaments from the continental shelf (Fisher, 1972; Kupferman and Garfield, 1977; Lillibridge III et al., 1990). From the surface to $\gamma^n = 27.7\,kg\,m^{-3}$ (~600 m depth, Fig. 4) the Labrador Current shows negative isoneutral slopes, indicative of westward flow. In the θ-S diagram (Fig. 5) the high density dots in the salinity range of 35.5–36 and temperature below 20 °C represents Slope Waters (SW), north of the GS (Lillibridge III et al., 1990). The Labrador Current brings Labrador Sea Water (LSW) between $27.8 < \gamma^n < 27.975\,kg\,m^{-3}$ (Fig. 4). This water mass has high values of CFC-11 and CFC-12 extending from 500 m to 1500 m depth in this area (Figs. 7 and 8). The LSW water masses are identified in the CFC-11 and CFC-12 vertical sections with values of approximately 2/2.8 pmol kg^{-1} and 1.2/1.6 pmol kg^{-1}, respectively for 2003/2012. The CFC signature in the LSW deepens to the range 900–2000 m south of the GS and extends southward, reaching Puerto Rico at intermediate levels.

Our section crosses the Gulf Stream (GS) at the latitudinal range ~37°–38.4°N. It is characterized by a steep slope in the isopycnals, indicating an eastward flow in the entire water column (Fig. 4). Immediately south of the GS the isopycnal slope changes sign. This change indicates the presence of the Gulf Stream Recirculation between ~35°–37°N, flowing to the west and occupying the entire water column.

The A22 section crosses the DWBC twice, once at the continental slope south of New England (~38°–39.5°N) and again north of Puerto Rico (~18.9°–19.9°N). On the northern side, the DWBC flows westwards from $\gamma^n = 27.7\,kg\,m^{-3}$ (nearly 600 m depth) to $\gamma^n = 28.1\,kg\,m^{-3}$ (~4500 m depth, Fig. 4). The location of the DWBC is more evident from the CFC vertical sections (Figs. 7 and 8) with two cores at about 800 m (approx. $\gamma^n = 27.8\,kg\,m^{-3}$) and 3000 m depth (about $\gamma^n = 28.05\,kg\,m^{-3}$) with values of approximately 2/2.8 pmol kg^{-1} and 1.6/1.8 pmol kg^{-1}, respectively, for CFC-11 in 2003/2012 and 1.4/1.6 pmol kg^{-1} and 0.6/0.8 pmol kg^{-1}, respectively, for CFC-12 in 2003/2012. High CFC concentrations are also observed north of Puerto Rico, where the deep flow is eastward from $\gamma^n = 27.875\,kg\,m^{-3}$ at approximately 1500 m depth to $\gamma^n = 28.1\,kg\,m^{-3}$ (~4000 m depth, Fig. 4). Here the DWBC is also observed through high silica (> 15 μmol kg^{-1}) and CFC concentrations at roughly 1500 m and 3500 m depth (Figs. 6–8), although the CFC signal is lower than that to the north of the GS. The CFC signals at intermediate depths (800 m to the north of the GS and 1500 m to the north of Puerto Rico) come from the LSW, while the deep signal (3000 m depth to the north of GS and 3500 m depth at Puerto Rico) comes from Iceland-Scotland Overflow Water (ISOW) and Denmark Strait Overflow Water (DSOW) (Smethie et al., 2000; Smethie, 1993), all together named Nordic Overflow Waters (NOW). North of Puerto Rico, the DWBC presents an uplift of the silica isolines at depths between 2500 and 4000 m in both cruises (Fig. 6). This is linked to the presence of Lower Deep Water (LDW), the mixing product of NOW with Antarctic Bottom Waters (AABW) (Van Aken, 2000; Hall et al., 2004; Joyce et al., 1999). The group of westward flowing water masses coming from the north and forming the DWBC (LSW, NOW and LDW) are called all together North Atlantic Deep Water (NADW). AABW is only found under the NADW near Puerto Rico (~18°N to 29.6°N), the deepest part of the section, where the approximate separating isoneutral is $28.14\,kg\,m^{-3}$ (Fig. 4). AABW is a cool ($\theta \leq 1.5$ °C, Fig. 3), fresh ($S < 34.87$, Fig. 4), high silicate (> 45 μmol kg^{-1}, Fig. 5) and low CFCs (CFC-11 < 0.2 pmol kg^{-1} and CFC-12 < 0.1 pmol kg^{-1} in both cruises, Figs. 5 and 6) water mass.

North of Puerto Rico, on top of the DWBC (~1200 m), the inclination of the isolines from the different properties indicates the presence of the Antilles current (19°–20.2°N in 2003 and 18.5°–19.5°N in 2012). This current flows westward from the surface to

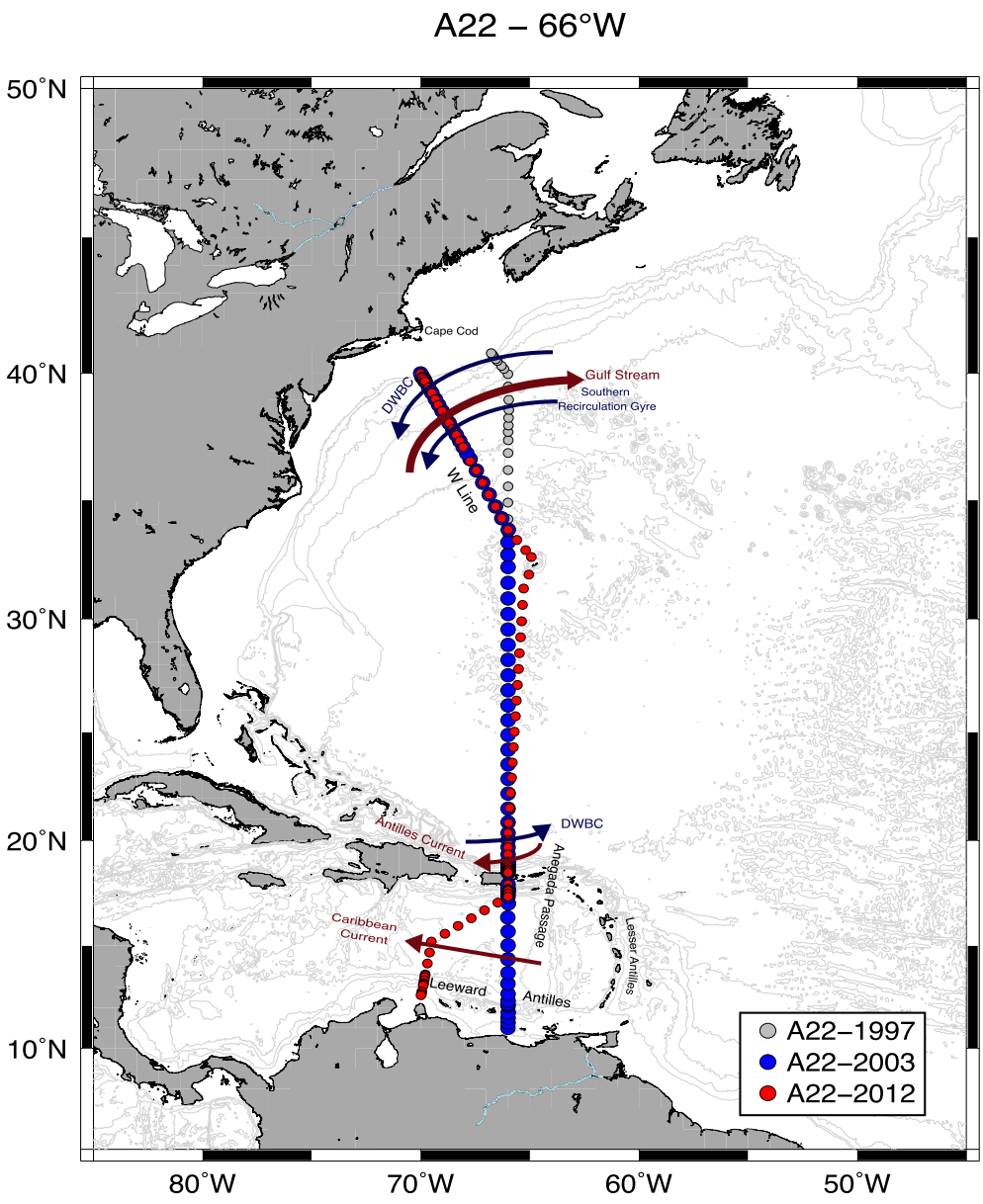

Fig. 1. Location of the hydrographic stations for A22 section and the main circulation patterns found in the section. Blue dots represent the 2003 stations, red dots the 2012 stations and the gray dots represent de 1997 stations. Blue arrows represent cold currents and red arrows warm currents. DWBC stands for Deep Western Boundary Current. Line W is part of the section that was surveyed previously various times in order to study the DWBC to the South of Cape Cod (Joyce et al., 2013). (For interpretation of the references to colour in this figure legend, the reader is referred to the web version of this article.)

approximately $\gamma^n = 27.7\,kg\,m^{-3}$ (Fig. 4).

The large amount of tracers found in the northern and southern sides of the basin depict a well-ventilated North Atlantic. In contrast, low CFCs are observed in the central part of the section (23°–27°N) under 2000 m depth, showing an area of old waters, not well exposed to the atmosphere (Joyce et al., 2001). The good ventilation in the northern part of the section, excluding the region between 23°N and 27°N, contrasts with the low degree of ventilation in the deep Caribbean, which has no connection with the North Atlantic below approximately 1700 m depth except for the Anegada Passage east of Puerto Rico (Joyce et al., 2001). The Anegada passage connection with the North Atlantic is detected by a signal of NADW characterized by low potential temperature (3.85 °C, Fig. 2) in the northern part of the Caribbean basin (~17°N) in the range of 2500 to 4500 m depth (Fig. 2). This recently ventilated NADW intrusion is also marked in both cruises by relatively low silica (< 29 μmol kg^{-1}, Fig. 6) and relatively high CFCs (CFC-11 in the range of 0.2 to 0.3 pmol kg^{-1} and CFC-12 between 0.1 and 0.2 pmol kg^{-1}, Figs. 7–8) at the northern edge of the basin (1700–3000 m depth). These anomalous values are greater in 2012 than in 2003, due to the NADW formed in the 1990s when the CFCs were introduced to the atmosphere were arriving to the Caribbean basin (LeBel et al., 2008). In the upper layer of the Caribbean above 100 m depth, a relatively freshwater water mass is found called Caribbean Surface Water (Fig. 3), formed by the mixture of North Atlantic Surface Waters and the complex processes of rainfall, runoff of the Amazon and Orinoco rivers and coastal upwelling (Hernández-Guerra and Joyce, 2000). As the 2012 cruise was carried out in spring, these surface waters are less stratified. Therefore, the salinity minimum due to freshwater inputs is less marked than in 2003 (Figs. 3 and 5). Below this fresh water mass, the North Atlantic Subtropical UnderWater (SUW) is seen, characterized by a salinity maximum (> 37) (Figs. 3 and 5). The SUW originates in the central tropical Atlantic, where the evaporation is higher than the precipitation (Metcalf, 1976). This water mass is only found at the northern part of the Caribbean, between 14°N and Puerto

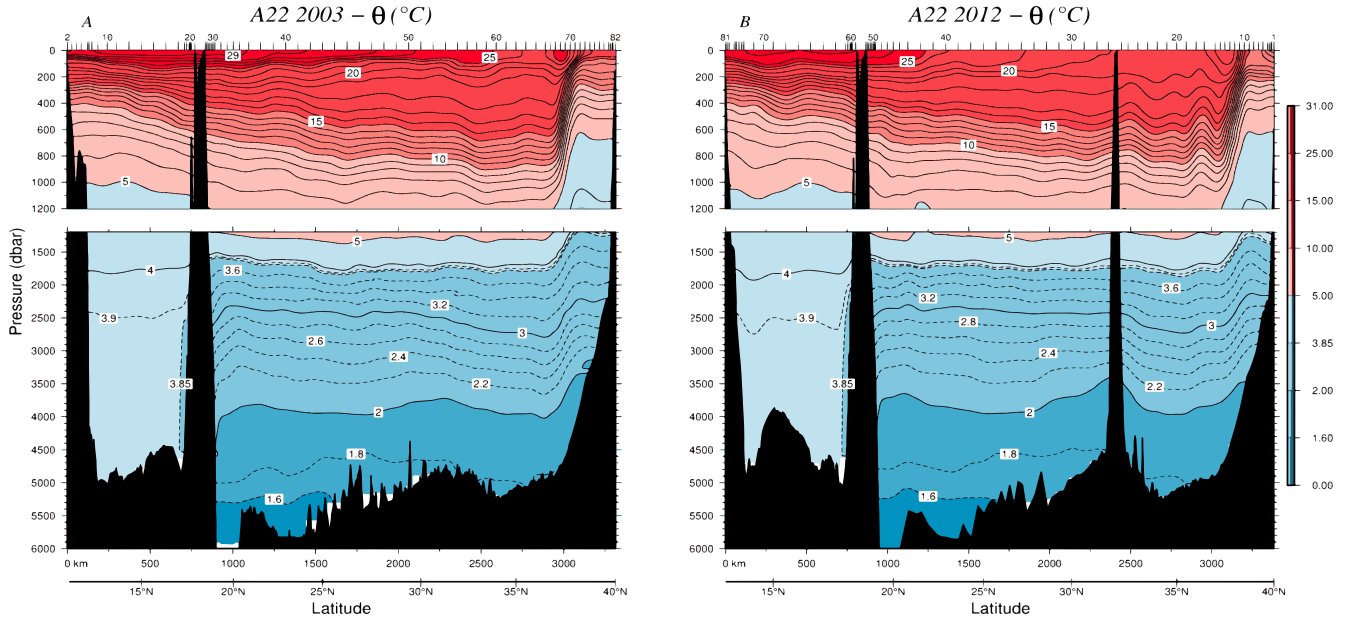

Fig. 2. Potential temperature vertical sections (°C). (A) for 2003 and (B) for 2012.

Rico. Between 300 and 500 m depth, the Tropical Atlantic Central Water is observed with lower salinity (< 36) (Fig. 3). Just below, between 500 and 900 m depth, there is a salinity minimum (< 35) corresponding with the Antarctic Intermediate Water (AAIW) which can be traced north of Puerto Rico at deeper depths (Metcalf, 1976).

3. Initial mass and silica transports

Before applying the inverse model, which imposes mass balance, an initial calculation of the geostrophic velocity at each station pair is done. To estimate the initial geostrophic transport, the thermal wind equation is used. The reference level of no motion is chosen at the depth of neutral density $\gamma^n = 28.14\,kg\,m^{-3}$ (dashed contour in Fig. 4) at approximately 5000 m depth, between the westward flowing LDW and the eastward flowing AABW. If a station pair is shallower than the reference layer, the deepest layer at this station is used as level of no motion. The mass transport is estimated between 17 neutral density layers defined as water mass boundaries following Joyce et al. (2001) (Table 1).

The initial (unbalanced) mass transports for 2003 and 2012 cruises are 37.0 Sv and 27.0 Sv, respectively (Fig. 9a and b). North of Puerto Rico, the whole Atlantic eastward mass transports are 63.3 Sv and 48.1 Sv for 2003 and 2012, respectively. In the Caribbean Sea, the westward mass transports are −26.3 Sv and −21.1 Sv for 2003 and 2012, respectively (Fig. 9a and b). From now on, positive transports are to the east and negative transports to the west. Qualitatively the unbalanced mass transports for both years have a similar structure through the water column.

The structure of the initial silicate transports (Fig. 9c and d), using the initial zero velocity geostrophic flow, has a similar structure to the initial mass transports. From layer 9 to the bottom all the net transport is due to the Atlantic part of the section as the Caribbean is an enclosed

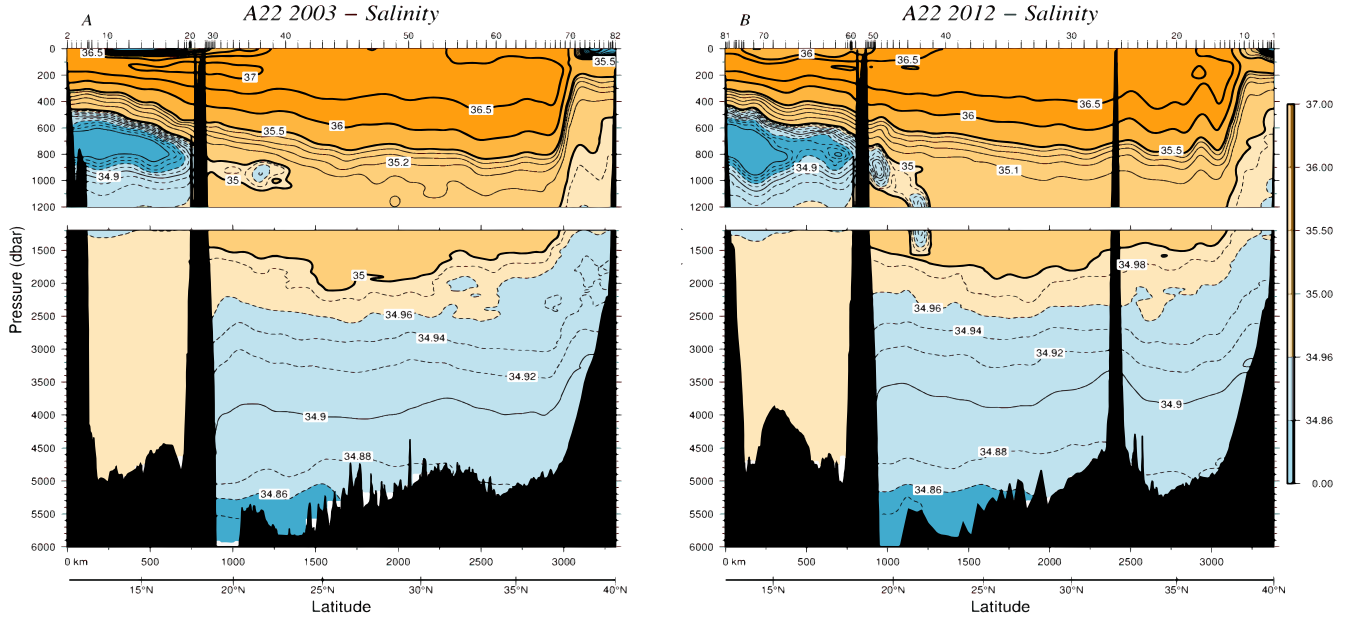

Fig. 3. Salinity vertical sections. (A) for 2003 and (B) for 2012.

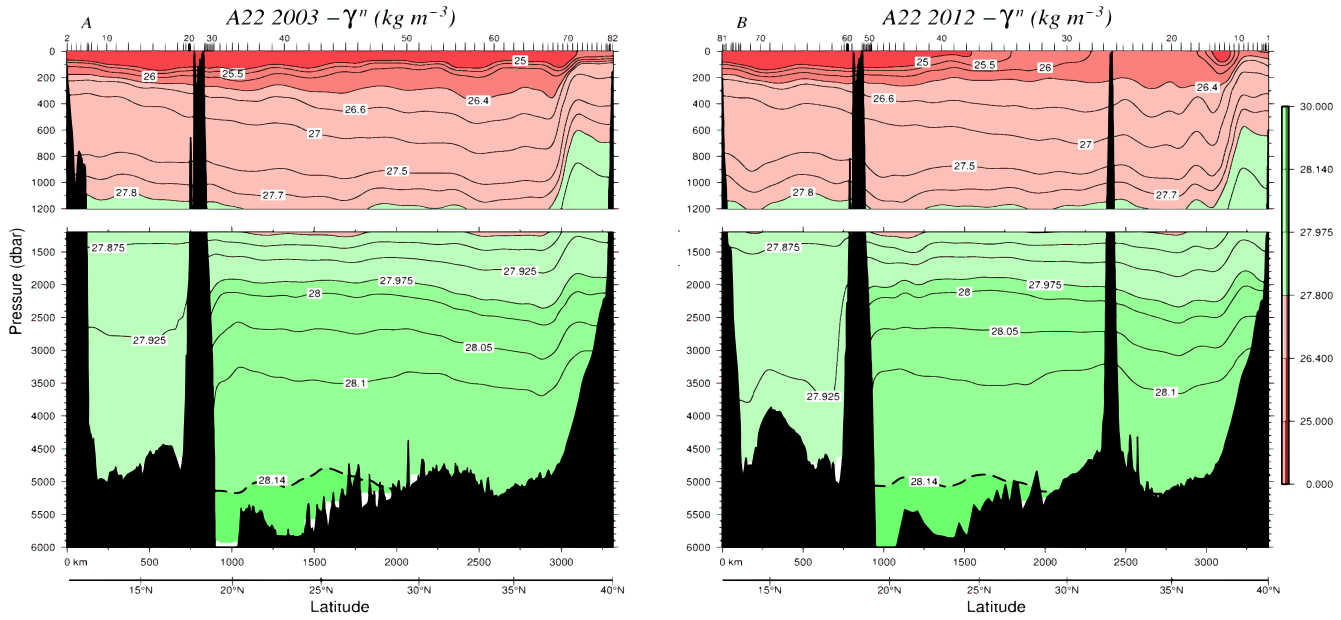

Fig. 4. Neutral density vertical sections (kg m^{-3}). (A) for 2003 and (B) for 2012. The dashed isopycnal indicates the reference layer of no motion for the initial transport.

basin at these depths. The silica transports structure at surface layers are different from those of the mass transport (Fig. 9a and b). The silica transport is almost zero due to the low silica concentration in the surface, while the mass transport is westwards in the Caribbean and eastward in the Atlantic between the densities $27 < \gamma^n < 27.7\,kg\,m^{-3}$. In both cruises, the silica flux of the Atlantic basin at the bottom and deep layers is high due to the high silica concentration in the AABW, LSW and NOW. The initial net silicate transport presents an imbalance of $566\,kmol\,s^{-1}$ in 2003 and $307.5\,kmol\,s^{-1}$ in 2012. These initial silica transports for the Atlantic are $718.3\,kmol\,s^{-1}$ and $468.9\,kmol\,s^{-1}$ for 2003 and 2012, respectively. For the Caribbean basin, the transports are $-152.3\,kmol\,s^{-1}$ and $-161.5\,kmol\,s^{-1}$ for 2003 and 2012, respectively.

4. Inverse box model solution

4.1. Mass constraints and LADCP-derived velocities

Inverse box models provide an efficient method to estimate the unknown geostrophic reference velocities for each station pair after obtaining the geostrophic flow using the thermal wind equation. These velocities at the reference layer per station pair are estimated by applying some constraints with certain uncertainties, of which the most important is mass conservation (Hernández-Guerra and Talley, 2016; Wunsch, 1996, 1978). Our inverse model also adjusts the Ekman transport included in the shallowest layer. Ekman transport is initially computed from NCEP wind stress interpolated to the location of each station pair where the geostrophic velocity is calculated (Ganachaud, 2003; Hernández-Guerra et al., 2014, 2010, 2005; Vélez-Belchí et al., 2017). The Ekman transport was estimated from the wind data during the period of the cruise following Hernández-Guerra and Talley (2016).

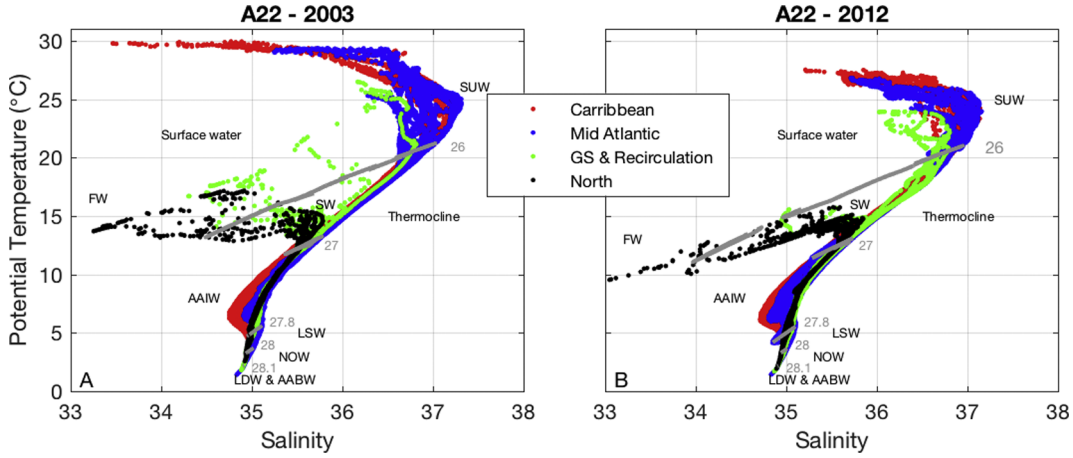

Fig. 5. θ-S diagram for both cruise years, (A) 2003 and (B) 2012. Grey lines indicate the selected neutral density layers of 25, 27, 27.8, 28 and 28.1 kg m^{-3} used in the inverse model. The colors of the dots indicated in the legend correspond with four main zones of the section. Red dots are for the Caribbean Sea, blue dots for the Mid Atlantic, green dots for the Gulf Stream and its recirculation and the black ones are for the region north of the Gulf Stream. Water masses are indicated with their acronyms: SUW stands for Subtropical UnderWater, FW stands for Ford Waters, SW stands for Slope Waters, AAIW stands for Antarctic Intermediate Waters, LSW stands for Labrador Sea Water, NOW stands for Nordic Overflow Waters, LDW stands for Lower Deep Waters and AABW for Antarctic Bottom Waters. (For interpretation of the references to colour in this figure legend, the reader is referred to the web version of this article.)

Table 1
Neutral density levels used in analysis (Joyce et al., 2001).

γ^n	Layer	Water Mass
20 – 25	1	Surface Layer
25 – 25.5	2	Upper thermocline
25.5 – 26	3	SUW
26 – 26.4	4	Upper thermocline
26.4 – 26.6	5	STMW
26.6 – 27	6	Lower thermocline
27 – 27.5	7	AAIW
27.5 – 27.7	8	AAIW
27.7 – 27.8	9	AAIW
27.8 – 27.875	10	ULSW
27.875 – 27.925	11	LSW
27.925 – 27.975	12	CLSW
27.975 – 28	13	ISOW
28 – 28.05	14	ISOW
28.05 – 28.1	15	DSOW
28.1 – 28.14	16	LDW
28.14 – 29	17	AABW

The initial Ekman transports are 0.2 ± 0.3 Sv in 2003 and -1.8 ± 0.4 Sv in 2012. After the inverse model, the Ekman transports are not significantly different than the initial values (0.2 ± 0.1 Sv in 2003 and -1.8 ± 0.7 Sv in 2012). In addition, LADCP data are used to adjust the geostrophic velocities prior to inverse modeling. The LADCP velocities from adjacent stations are averaged and compared to the geostrophic velocity profile of each station pair: the depth intervals over which the vertical velocity profiles have similar structures are used to estimate the reference velocity at each station pair (Fig. 10), following Comas-Rodríguez et al. (2010). These adjustments were done for 57 station pairs in 2003 cruise and for 49 stations pairs in 2012 cruise.

We apply the inverse model to the volume enclosed between the hydrographic stations of the A22 section and the American continent to the west as there is no major flow through the Panama Canal (Joyce et al., 2001). We have carried out two different inverse models. Model A includes the total mass conservation (constraint 1), the mass conservation per neutral density layer of Table 1 (constraints 2 to 18), with the adjustment of the Ekman transport included in the shallowest layer and the total mass conservation, and a constraint of 0 ± 0.5 Sv at the deep Caribbean from layers 11 to 17 (constraint 19). Model B also includes silicate conservation (constraints 20 to 37, Section 4.2). These constraints together with their error are the set of initial equations forming the following matrix equation:

$$Ab + n = -Y \quad (1)$$

where A is an $M \times N$ matrix, M is the number of layers and constraints and N the unknowns, b is a column vector of length N containing the unknown velocities at the reference layer of N station pairs, n is a column vector of length M with the noise of each layer and constraint, and Y is a vector representing the mass transport initially imbalanced in each layer.

To solve the inverse problem, which has more unknowns than equations, the Gauss–Markov method is applied which produces a minimum error variance solution from the initial estimates of the unknowns (Wunsch, 1996). Therefore, this method requires preliminary variance for each constraint and for each velocity. The a priori equation variance and velocity variance used are those from Joyce et al. (2001). For the a priori equation variance we have chosen higher variance in the surface than in the deeper layers. These values are $(2\,\text{Sv})^2$ for the first 5 constraints which include the total and the first four layers; $(0.5\,\text{Sv})^2$ for the bottom layer and $(1\,\text{Sv})^2$ for the rest of the constraints. The velocity variance used is higher for those station pairs that do not have LADCP measurements, $(0.1\,\text{m s}^{-1})^2$, than for those with LADCP measurements, $(0.05\,\text{m s}^{-1})^2$.

After the inverse calculations, we have used the new reference velocities to calculate the new mass transports. Fig. 11a-b shows the meridionally integrated mass transport for the Atlantic Ocean, Caribbean Sea and the net transport of the entire section, for both years. In this figure, the net mass transport from layer 9 to the bottom is almost zero. At the surface layers, there is a net westward inflow in the Caribbean sub-basin and a net eastward outflow in the Atlantic sub-basin of our section.

4.2. Silica constraints

In order to improve our results, we carried out a Model B using silica fluxes as constraints in our inverse calculations. The net silica fluxes after the inverse model with mass constraints (Model A, Fig. 11c–d) show different patterns compared to mass fluxes (Fig. 11a-b) especially in the surface and bottom layers. Therefore, we added 18 new equations, considering silica conservation as constraints, to our 19 mass

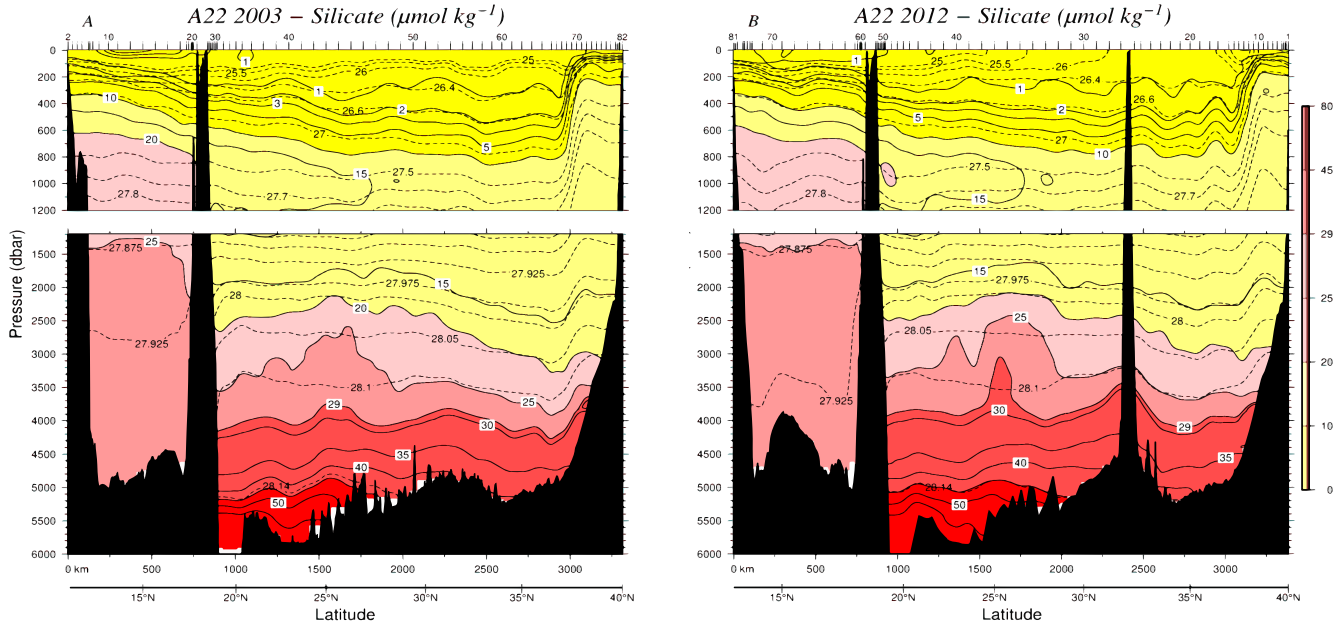

Fig. 6. Silica vertical sections (μmol kg^{-1}). Dashed lines show the neutral density contours and solid lines for silica contours. (A) for 2003 and (B) for 2012.

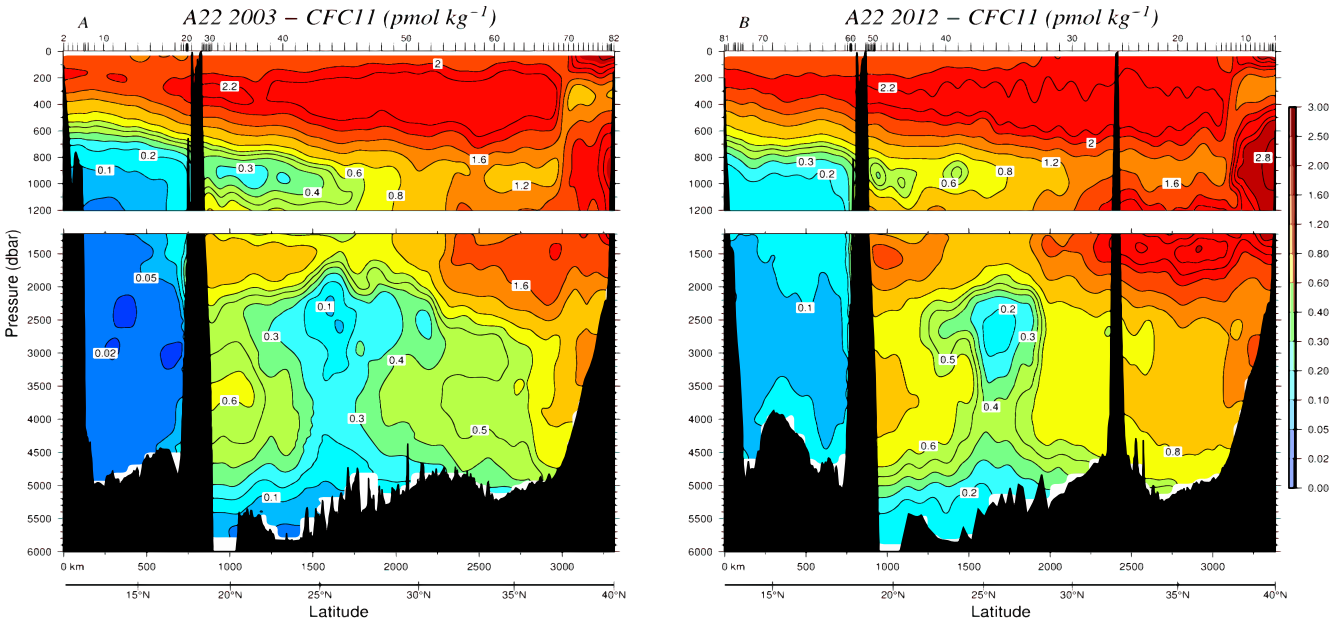

Fig. 7. CFC-11 vertical sections in pmol kg^{-1}. (A) for 2003 and (B) for 2012.

conservation equations. The *a priori* variances used are those used by Joyce et al. (2001). These variances are (20 kmol s^{-1})^2 for the first four layers, (5 kmol s^{-1})^2 for the total silica conservation and the last two layers and (10 kmol s^{-1})^2 for the rest of the constraints.

The reference velocity adjustments to the initial LADCP-based geostrophic velocity as function of latitude estimated from the inverse model with the silica and mass constraints and for the inverse model with only mass constraints are shown in Fig. 12. The differences between the reference velocities adjustments before and after applying the silica constraints only differ by less than 2 cm s^{-1} but eliminates much of the silica imbalances. These reference velocities are small in the central part of the section where there is not any major flow or current. In the Caribbean in 2003 the values at the southern part are negative and at the northern part are positive, as the inverse model results are trying to decrease the cyclonic gyre of the Caribbean basin. In 2012 data, the cyclonic pattern in less marked, but it still appears with high negative velocities at 16°N. North of Puerto Rico the deep water eastward flow increases in 2012, while between 20°N and 25°N the westward flow increases in both years.

Fig. 13 shows the LADCP-adjusted geostrophic velocities and the LADCP-adjusted velocities adding the reference velocities for both inverse solutions (Model A and B). The velocities of both models, A and B, are very similar, except for the velocities in the range of latitudes 27° to 28°N in 2003, which in model A are more negative. Comparing the LADCP-adjusted geostrophic velocities to those of both models, the velocities are similar, but in 2003 the inverse model has made the flow in the Caribbean negative as in the middle part of the section while in the northern part of the Gulf Stream (~39°N) the flow has been made positive. In 2012, the inverse model has also made the Caribbean flow more negative, but to the north of Puerto Rico the flow is more positive than in the only LADCP-adjusted velocities. The velocities adjusted from Model B are used to calculate the new mass, silica and heat

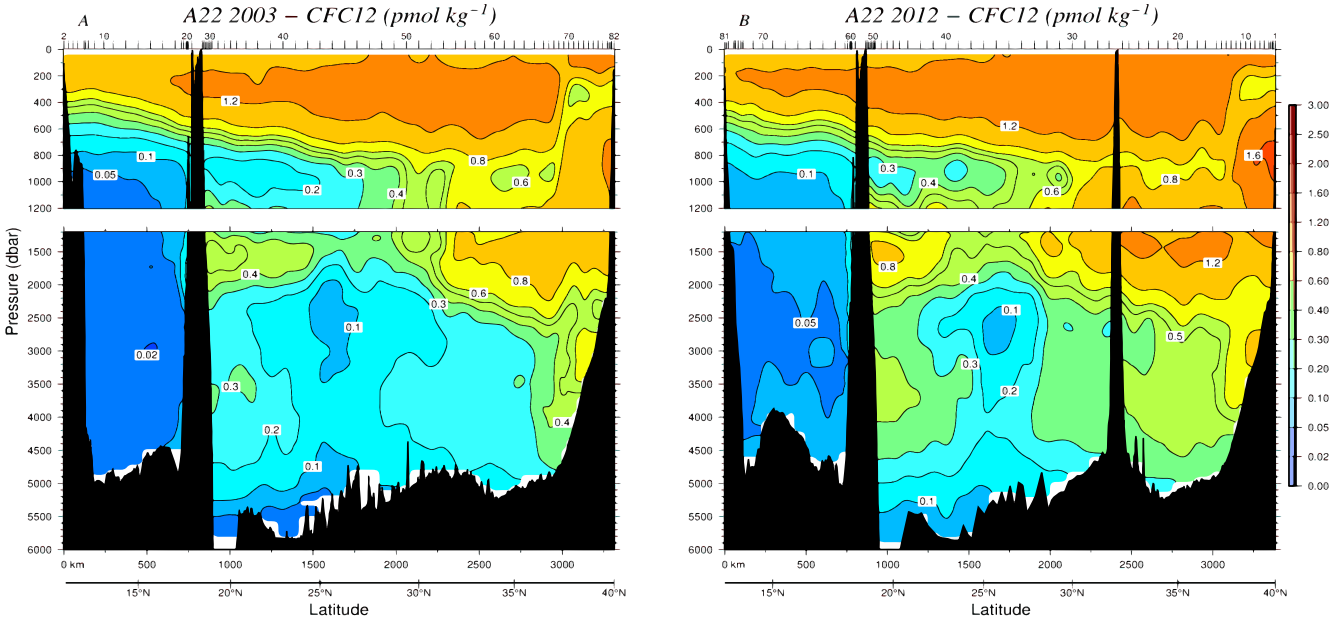

Fig. 8. CFC-12 vertical sections in pmol kg^{-1}. (A) for 2003 and (B) for 2012.

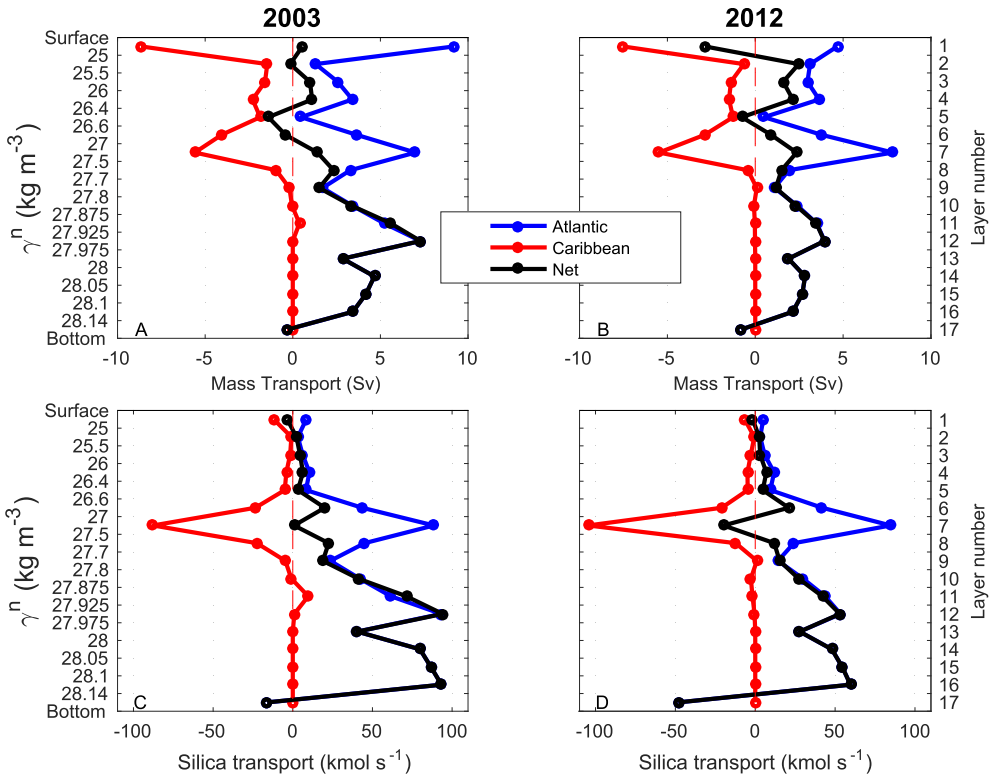

Fig. 9. Initial (unbalanced) meridionally integrated mass and silica transports across the A22 section. Relative to zero velocity at neutral density $\gamma^n = 28.14\,\mathrm{kg\,m^{-3}}$. (A) and (B) show for 2003 and 2012 mass transports (Sv) and (C) and (D) show 2003 and 2012 silica transports (kmol $\mathrm{s^{-1}}$). Black lines are the net transport, the blue lines are the Atlantic part of the section (from Puerto Rico to Cape Cod, USA) and red lines are the Caribbean part of the section. (For interpretation of the references to colour in this figure legend, the reader is referred to the web version of this article.)

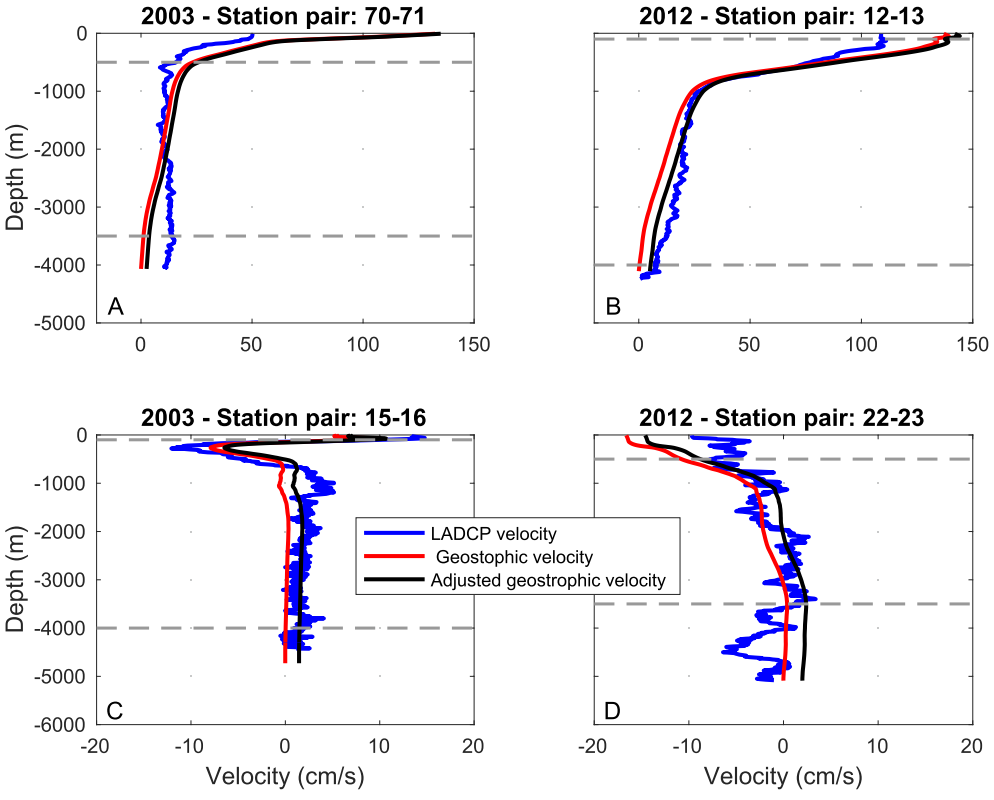

Fig. 10. Examples of the LADCP velocity profiles used to reference the geostrophic velocity (cm $\mathrm{s^{-1}}$). LADCP normal to station pair (blue), geostrophic velocity referred to the initial level of no motion (red) and LADCP adjusted geostrophic velocity (black) with the depth interval used to make LADCP adjustments between the horizontal grey dashed lines. The selected station pairs are (A) Gulf Stream 2003 and (B) 2012, (C) Caribbean 2003, and (D) Gulf Stream Recirculation 2012. (For interpretation of the references to colour in this figure legend, the reader is referred to the web version of this article.)

transports.

Mass and silica meridionally integrated transports from the inverse calculations with mass and silica constraints for 2003 and 2012 are shown in Fig. 14. The net mass and silica transports for 2003 (2012) are -0.2 ± 1.6 Sv (0.3 ± 2.0 Sv) and $14.8 \pm 22.3\,\mathrm{kmol\,s^{-1}}$ ($-2.5 \pm 22.6\,\mathrm{kmol\,s^{-1}}$), respectively. In both years, the net silica transport has been reduced considerably from those transports estimated from the inverse model with only mass constraints. The inverse calculations with mass and silica constraints have improved the balance of silica transports in the deep and bottom layers (compare Fig. 14c–d with 11c–d).

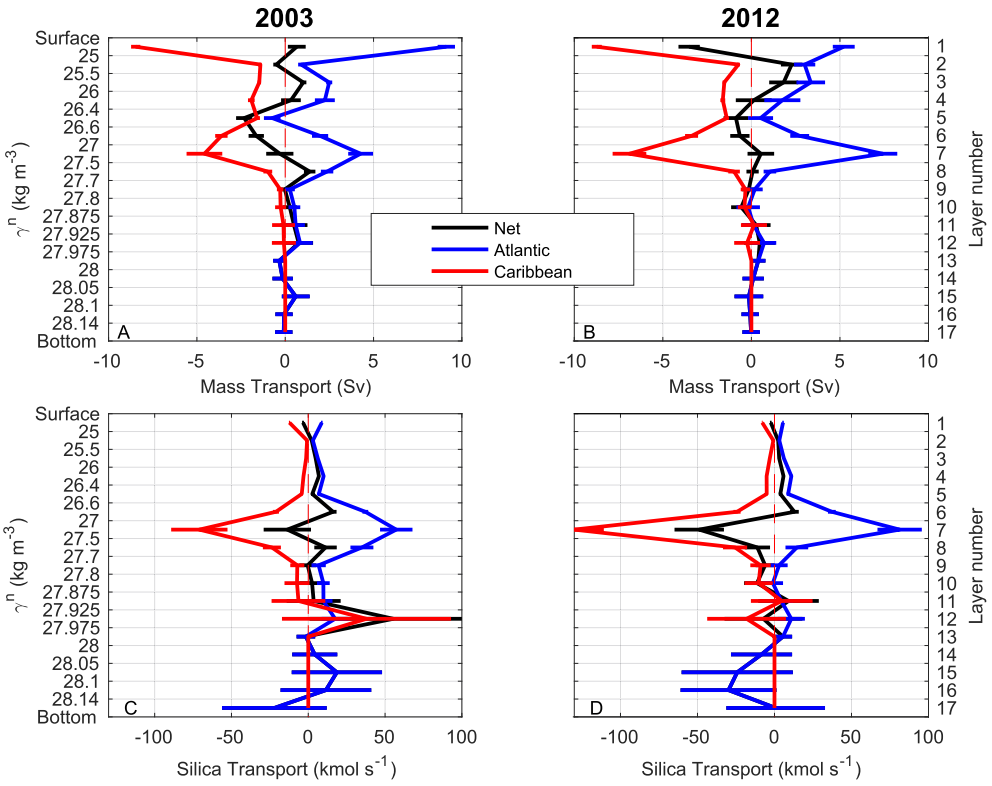

Fig. 11. Mass and silica transports after the inverse model solution with mass constraints (Model A). Red line stands for the Caribbean Sea mass transport, blue line is for the Atlantic mass transport and black line is for the entire section mass transport. (A – C) and (B – D) are 2003 and 2012 cruises, respectively. (For interpretation of the references to colour in this figure legend, the reader is referred to the web version of this article.)

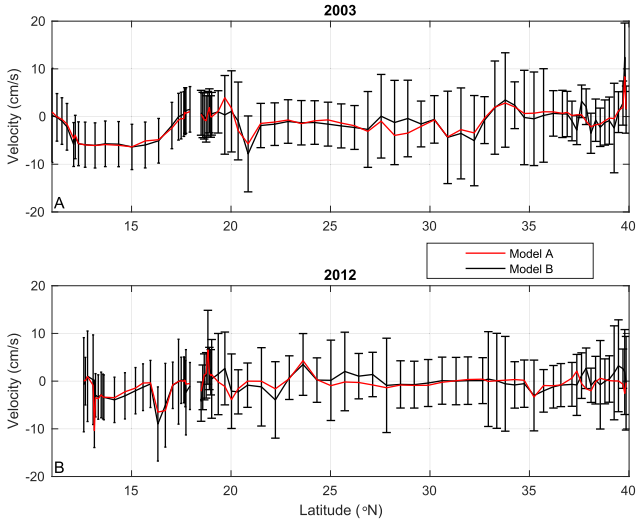

Fig. 12. Velocity at the reference layer as function of latitude determined by the inverse model calculations for 2003 (A) and 2012 (B). Red lines are for inverse model A. Black lines with error bars correspond to inverse model B. The gap in the velocity plots is due to the island of Puerto Rico. (For interpretation of the references to colour in this figure legend, the reader is referred to the web version of this article.)

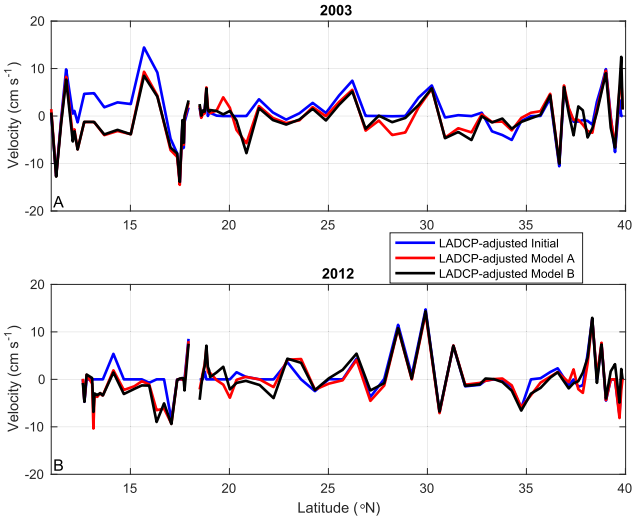

Fig. 13. LADCP-adjusted geostrophic velocities as a function of latitude (blue line), LADCP-adjusted velocities plus the reference velocities estimated from the inverse calculations using mass constraints (Model A, red line) and LADCP-adjusted velocities plus the reference velocities estimated from the inverse calculations using mass and silica constraints (Model B, black line). (For interpretation of the references to colour in this figure legend, the reader is referred to the web version of this article.)

5. Adjusted geostrophic transports

The mass transports after the inverse model with mass and silica constraints from each year and at different locations and layers are shown in Table 2. The final net transports are −0.2 ± 1.6 Sv and 0.3 ± 2.1 Sv for 2003 and 2012, respectively. In the Caribbean the net flow is westwards in both years as Centurioni & Niiler (2003) and Joyce et al. (2001) described. The negative transports in the Caribbean are −24.4 ± 1.0 Sv in 2003 and −24.2 ± 1.1 Sv in 2012 (Table 2), not significantly different than the net transport estimated by Joyce et al. (2001) in 1997, who found westward transport of 24 Sv. Most of these westwards transports in the Caribbean are due to the thermocline and intermediate transport. At these layers, 3 westward jets are seen in 2003 (Fig. 15), one at ~12°N, other at ~16°N and the last at ~18°N, very close to the southern coast of Puerto Rico. These jets are wind-driven structures (Hernández-Guerra and Joyce, 2000) intensified by salinity gradients produced by freshwater inputs from the coastal upwelling and the runoff of the Orinoco and Amazon rivers between August and December (Chérubin and Richardson, 2007). In 2012 as the

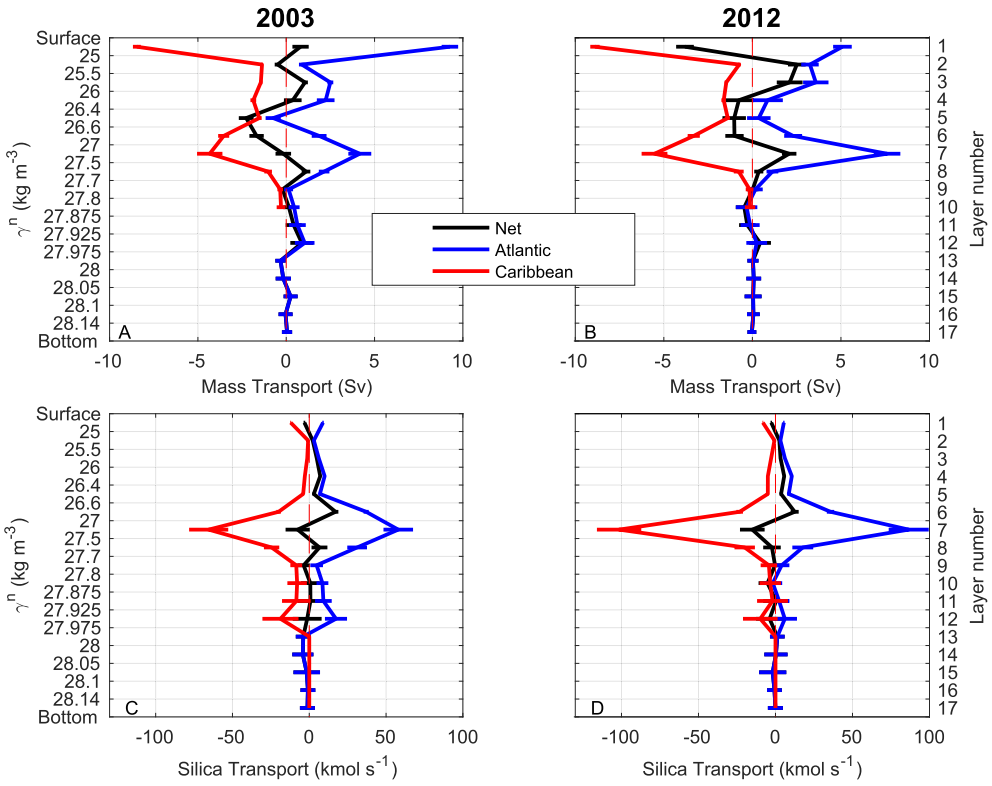

Fig. 14. Meridionally integrated mass and silica transports after the inverse model solution with mass and silica constraints (Model B). Black lines are the net transport, blue lines the Atlantic transports and red lines the Caribbean transports. Left subplots corresponds to 2003 and right ones to 2012. The top subplots correspond with mass transports (Sv) and the bottom subplots with the silica transports (kmol s^{-1}). (For interpretation of the references to colour in this figure legend, the reader is referred to the web version of this article.)

cruise was carried out in spring, when the stratification is low and the fresh water input is less, only 2 jets at ~12°N and ~17°N are seen as Chérubin and Richardson (2007) reported. The two deepest layers of the Caribbean do not have any net flux because the Caribbean is isolated at depth greater than 1700 m as seen in the horizontal distribution of the meridional transport between the different density layers (Fig. 16f and g). The deep flow of the Caribbean is restricted to layers 10 and 11, as layer 12 does not exist in the Caribbean Basin. In 2003, this deep layer shows a cyclonic gyre of 11.3 ± 6.8 Sv at the southern part (~10–14°N) and 2 little anticyclonic gyres of 9.4 ± 10.1 Sv and 9.9 ± 5.3 Sv at the northern part at ~14°–16°N and 16°–18°N, respectively (Fig. 16e). Typically, the deep Caribbean contains a cyclonic gyre (Hernández-Guerra and Joyce, 2000; Sou et al., 1996), as observed in 2012. This cyclonic gyre transport is about 15.2 Sv, (Fig. 16e).

The surface Antilles Current flows westwards close to the shore north of Puerto Rico. This current has a large temporal variability, varying in the range of −15 to +25 Sv in the upper 1000 m in period ranged between March 2004 and May 2005 (Bryden et al., 2005; Johns et al., 2008). In 2003, the Antilles Current flows at ~100 km away from the northern shore of Puerto Rico (19.0°–20.2°N, Fig. 15a) carrying −9.2 ± 3.1 Sv. In contrast, in 2012, the Antilles Current flows close to Puerto Rico (18.5°–19.6°N, Fig. 15b) transporting −15.9 ± 2.0 Sv.

Also to the north of Puerto Rico, between 18.7°–21.2°N in 2003 and 18.7°–20.2°N in 2012, the DWBC flows to the east (Figs. 15 and 16e, f and g). This eastward flow is divided into 3 main parts, the LSW layer (isoneutral layers 10 to 12, in the range of 1500 to 2000 m depth) which transports 9.0 ± 2.5 Sv in 2003 and 6.6 ± 2.0 Sv in 2012; the NOW layer (isoneutral layers 13:15, between 2100 and 3700 m depth) which transports 12.7 ± 4.6 Sv in 2003 and 7.7 ± 3.6 Sv in 2012; and the deepest layer, the LDW layer (isoneutral layer 16, from 3700 to

Table 2
Regional inverse model transports with mass and silica constraints (Model B) for A22 in 2003 and 2012. Positive transports are eastward.

	Latitude (°N)		Layers	Transports	
	2003	2012		Model B 2003	Model B 2012
Upper North DWBC	38.0–39.6	38.4–39.6	10:12	−9.7 ± 1.9	−9.5 ± 1.8
Lower North DWBC	38.0–39.6	38.4–39.6	13:15	−6.1 ± 1.7	−4.9 ± 1.6
LDW North	38.0–39.6	38.4–39.6	16	−1.5 ± 1.5	−0.5 ± 0.5
Net North DWBC	38.0–39.6	38.4–39.6	10:16	−17.3 ± 2.9	−14.9 ± 2.5
Gulf Stream	37.0–38.0	37.3–38.4	1:17	100.1 ± 4.6	123.8 ± 4.4
Gulf Stream Recirculation	35.0–37.0	36.0–37.3	1:17	−59.8 ± 8.8	−43.0 ± 10.9
Upper South DWBC	18.7–21.2	18.7–20.2	10:12	9.0 ± 2.5	6.6 ± 2.0
Lower South DWBC	18.7–21.2	18.7–20.2	13:16	12.7 ± 4.6	7.7 ± 3.6
LDW South	18.7–21.2	18.7–20.2	16	9.2 ± 8.9	3.3 ± 7.5
Net South DWBC	18.7–21.2	18.7–20.2	10:16	30.9 ± 10.3	17.6 ± 8.6
AABW	18.5–29.22	18.5–29.7	17	0.1 ± 0.3	0.03 ± 0.27
Antilles	19.0–20.2	18.5–19.6	1:9	−9.2 ± 3.1	−15.9 ± 2.0
Caribbean	11.1–17.8	12.6–17.8	1:9	−23.9 ± 0.9	−23.9 ± 0.9
			10:11	−0.5 ± 0.5	0.3 ± 0.5
			1:11	−24.4 ± 1.0	−24.2 ± 1.1
Net	11.1–40.0	12.6–40.0	1:17	−0.2 ± 1.6	0.3 ± 2.1

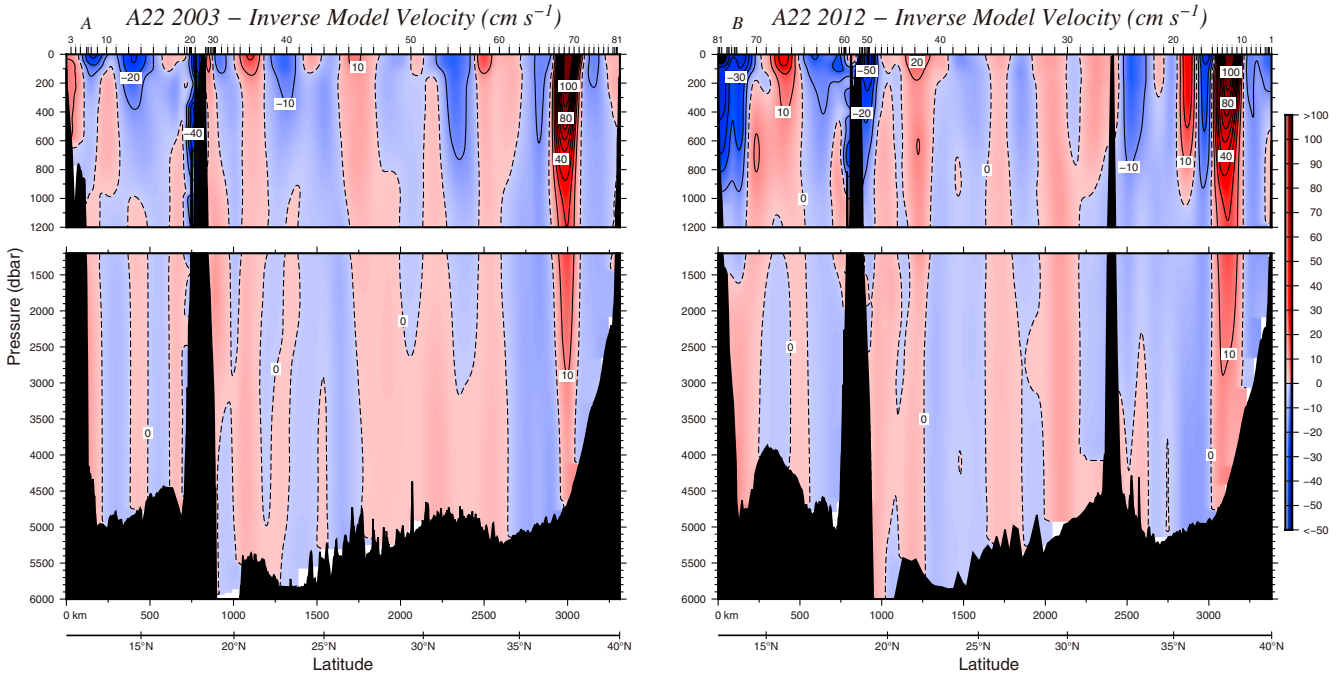

Fig. 15. Geostrophic velocities normal to the section A22 after the inverse model with mass and silica constraints and LADCP adjusted (cm s^{-1}). Positive velocities (red) are to the east and negative velocities (blue) to the west. (A) for 2003 and (B) for 2012. (For interpretation of the references to colour in this figure legend, the reader is referred to the web version of this article.)

5200 m depth) which transports 9.2 ± 8.9 Sv in 2003 and 3.3 ± 7.5 Sv in 2012. Thus, the net DWBC transports are 30.9 ± 10.3 Sv and 17.6 ± 8.6 Sv in 2003 and 2012, respectively. Both of these transports match with the DWBC transports estimated by Hernández-Guerra et al. (2014) at 7.5°N in 1993 (30.8 ± 3.1 Sv southward) and in 2012 (18.4 ± 3.6 Sv southward). North of the DWBC, between ~24° and 27°N, the layers 10 to 16 have westward flow (Fig. 16). This flow carries the less ventilated waters of the section, presenting low CFCs and high silica (Figs. 6–8), and which appear to be disconnected from the deep boundary current (Hall et al., 2004; Steinfeldt et al., 2007). From north of 27°N to the Gulf Stream Recirculation there are ventilated waters with some westwards/eastwards oscillations attributed to eddies (Fig. 16).

The GS and its recirculation are observed between ~35°–38.4°N, south of the Northern Recirculation Gyre (NRG) (Fig. 16). Hogg (1992) observed an increase of 20–30 Sv downstream in the GS due to the water entrainment from the NRG. The GS carries 100.1 ± 4.6 Sv in 2003 and 123.8 ± 4.4 Sv in 2012 eastward, of which −59.8 ± 8.8 Sv in 2003 and −43.0 ± 10.9 Sv in 2012 recirculate immediately south of it (Table 2). The difference in transports between the 2003 and 2012 recirculation is due to the presence of a Cold Core Ring (CCR) south of the GS in 2012 (Fig. 16). The CCR is identified by the presence of Eighteen Degree Water (EDW) defined by T ~ 18 °C and S ~ 36.5 (Worthington, 1959). The CCR is observed at around 36°N in the vertical sections of potential temperature (Fig. 2), salinity (Fig. 3), neutral density (Fig. 4), silica (Fig. 6) and velocity (Fig. 15). Another possibility for the differences observed between both cruises is that the GS has higher transports in winter/spring than in summer/fall (Sato and Rossby, 1995). The 1997 section ran meridionally from Cape Cod at 66°W and did not follow the W line as in 2003 and 2012. Thus, the higher GS transport in 1997 (153–158 Sv, Joyce et al., 2001) in contrast to that of 2003 is probably explained by the water entrainment from the NRG.

Between the northern edge of the GS and the northern boundary of the section, LSW is carried in the upper part of the DWBC at a depth range of 700 to 1900 m (layers 10 to 12). At these depths, the westward transport is −9.7 ± 1.9 Sv and −9.5 ± 1.8 Sv in 2003 and 2012, respectively (Table 2). The lower part of the DWBC transports NOW between 1900 and 3000 m depth (layers 13 to 15). The NOW fluxes are −6.1 ± 1.7 Sv/−4.9 ± 1.6 Sv in 2003/2012. Hernández-Guerra et al. (2014) observed an increase/decrease in the transport of the LSW/NOW between 1992 and 2011 at 7.5°N and 24.5°N. The LSW and NOW transports of the DWBC, between 2003 and 2012 in the A22, do not present any significant change. At the deepest layer of the NADW (from 3000 m depth to the bottom, layer 16) LDW transports −1.5 ± 1.5 Sv/−0.5 ± 0.5 Sv in 2003/2012. Therefore, net transport of the northern DWBC is −17.3 ± 2.9 Sv in 2003 and −14.9 ± 2.5 Sv in 2012. Macdonald (1998) estimated similar transports of the DWBC of −14 ± 5 Sv at 36°N and Ganachaud (2003) of −16 ± 2 Sv at 48°N. This transport introduces the new ventilated waters to the western tropical Atlantic (Joyce et al., 2001). In 2003, the transport of the DWBC in the south section is higher (by ~13 Sv) than in the north section possibly due to the entrainment of water masses along the path of the DWBC between both latitudes.

6. Heat and freshwater fluxes

We now consider the heat and freshwater fluxes for the volume enclosed to the west of 66°W. Our final mass transport solution (Fig. 14 a and b) indicates a net inflow of surface warm waters in 2012, which leads to an outflow in layer 2, suggesting a transformation of surface waters into thermocline waters which are transported out of the box used in the model. Meanwhile, this transformation does not occur in 2003. The variation in the formation of thermocline waters and inflow/outflow of surface waters is marked by seasonal changes as the cruise carried out in 2012 was in early spring when the surface layer is cooler. A transformation of the Subtropical Mode Water into EDW and Slope Waters in between layers 3 and 6 occurs in the northern edge of the Mid Atlantic Bight. During the transformation process, these waters are transported westwards through the southern edge of the GS. The region between the shelf front south of New England and the GS during winter is cooled in the upper 150 m producing a water mass with temperature and salinities in between 10–13 °C and 34.8–35.6, respectively. This water flows in the layers 7 and 8, generally westwards, but occasionally

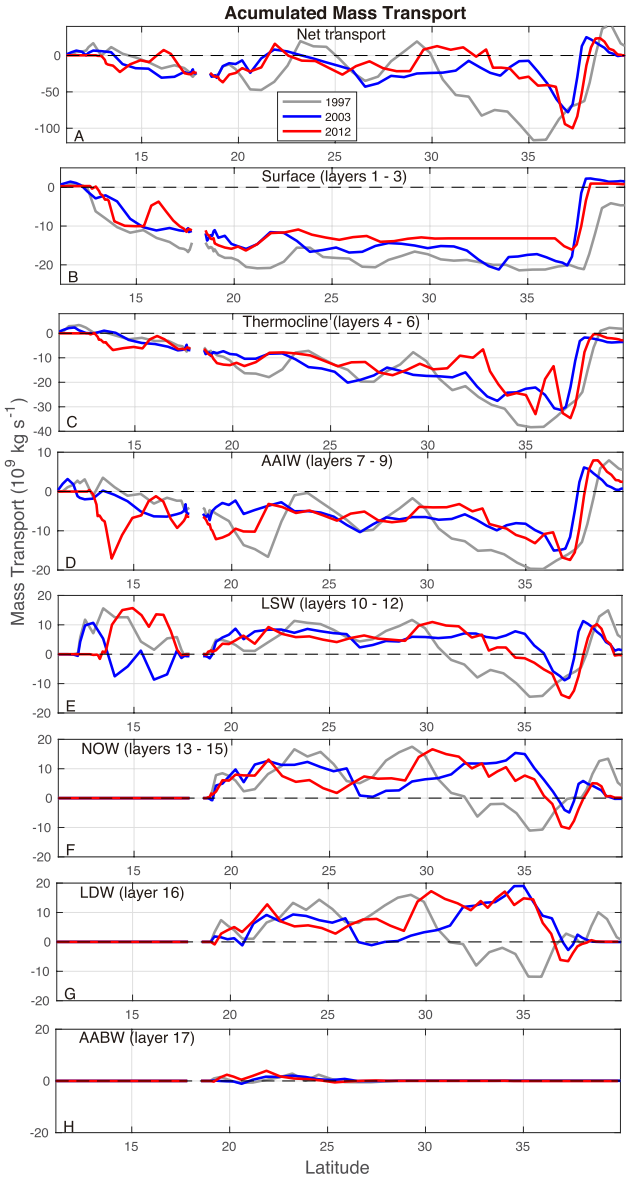

Fig. 16. Integrated mass transports (Sv) after Model B for the three years (gray line for 1997, blue line for 2003 and red line for 2012). Subplot (A) is the net transport (layers 1 to 17), (B) is the surface transport (layers 1 to 3), (C) is the thermocline transport (layers 4 to 6), (D) is the Antarctic Intermediate Waters (layers 7 to 9), (E) is the Labrador Sea Waters (layers 10 to 12), (F) is the Nordic Overflow Waters (layers 13 to 15), (G) is the Lower Deep Water (layer 16) and (H) the Antarctic Bottom Water (layer 17. (For interpretation of the references to colour in this figure legend, the reader is referred to the web version of this article.)

flows eastwards in the GS and as part of the northern recirculation gyre (Joyce et al., 2001). This water mass outflow is clearly seen in the layer 7 in 2012.

Using the inverse model with mass and silica constraints we have estimated a net heat exchange through our section of −0.23 ± 0.08 PW and −0.21 ± 0.12 PW in 2003 and 2012, respectively. The negative sign implies that heat is transported westward across A22 where it is lost to the atmosphere. Comparing our heat loss to the atmosphere (roughly 0.20 PW) to Hall et al. (2004) (0.45 PW), our heat transport is smaller due to the smaller area used to the west of the section than that of the 52°W line, which is east of A22 and therefore inclusive of the major wintertime heat loss to the atmosphere (Joyce et al., 2013). However, our net heat flux is similar to that of Joyce et al. (2001) for our same section (−0.25 PW).

The freshwater flux inflow/outflow of our section should be the balance between evaporation and precipitation plus the runoff. We have followed the procedure of Joyce et al. (2001) where the freshwater flux (F) is estimated from the mass transport of our inverse model B and the salinity as follows: $F = \sum_i \sum_j T_{ij} S'_{ij} / S_0$, where T_{ij} is the matrix of mass transport with i layers and j station pairs. S_0 is the mean salinity and S'_{ij} is defined from the salinity of each layer and station pair, as $S'_{ij} = S_{ij} - S_0$. We have used two different mean salinities to estimate the freshwater flux. The first one is that obtained from our salinity data from both cruises. The other one is the global mean salinity of 34.9 estimated by Talley (2008).

For our enclosed area, the freshwater fluxes are −0.32 Sv in 2003 and 0.24 Sv in 2012 from the section mean salinity. The fluxes estimated from the global mean salinity are similar to those obtained from the section mean salinity, being −0.33 and 0.25 for 2003 and 2012, respectively. A positive flux means that evaporation (E) is higher than precipitation (P) and runoff. The freshwater flux estimated by Joyce et al. (2001) for the same section but in 1997 is in the range of 0.31–0.37 Sv. The results with opposite sign could indicate that the precipitation/evaporation ratio in the region varies seasonally. The 1997 cruise was carried out in summer when the highest evaporation occurs. The 2012 cruise was done during spring when the evaporation also dominates over the precipitation and runoff. Finally, the 2003 cruise was performed in fall, the rainy season, and the period of the year when the greatest input of fresh water from the Amazon and Orinoco rivers takes place (Chérubin and Richardson, 2007). To compare the precipitation rates from the three cruises, the accumulated precipitation during the period of each cruise was calculated from NCEP precipitation data (Kalany et al., 1996). The amount of precipitation during the 2003 cruise was double the precipitation amount of the other two cruises (16.9 g m^{-2} s^{-1} in 1997, 32.2 g m^{-2} s^{-1} in 2003 and 17.4 g m^{-2} s^{-1} in 2012).

7. Discussion

The westward flow in the Caribbean, produced at the thermocline and intermediate layers, is similar in 1997, 2003 and 2012 cruises (~24 Sv, Fig. 16 and Table 2). In the Caribbean basin there are some westward wind-driven jets at the surface and thermocline layers as described in Hernández-Guerra & Joyce (2000) that vary seasonally in number and intensity depending on the freshwater inputs (Chérubin and Richardson, 2007). In 1997, Hernández-Guerra and Joyce (2000) described a unique westward jet at 13°N. In 2003 and 2012, three (12°N, 16°N and 18°N) and two (12°N and 17°N) jets, respectively, were identified (Fig. 15). This number of jets coincides with the seasonal variability observed by Chérubin and Richardson (2007). In the deepest layers of the Caribbean (10–11), different features are observed in 2003 and 2012 (Fig. 16e). In 2012, a unique cyclonic gyre transporting 15.2 ± 8.7 Sv is seen that is not apparent in 2003. This transport is similar to the transport of the cyclonic gyre in 1997 (~15 Sv, Joyce et al., 2001). The relatively high CFC concentration at the bottom and northern edge of the Caribbean basin observed by Joyce et al. (2001) increased from 1997 to 2012. CFCs enter the Caribbean as NADW overflows through the Anegada Passage. The bottom CFCs remained at low values in 1997 and 2003 (~0.05 pmol kg^{-1} for both, CFC-11 and CFC-12, Figs. 7–8). Nevertheless, in 2012, the bottom CFCs increased to 0.2 pmol kg^{-1} and 0.1 pmol kg^{-1} for CFC-11 and CFC-12, respectively. At the northern boundary (DWBC overflow), the CFCs increased 0.1 pmol kg^{-1} at each cruise. These values are 0.1 pmol kg^{-1}, 0.2 pmol kg^{-1} and 0.3 pmol kg^{-1} for CFC-11 in 1997, 2003 and 2012, respectively. CFC-12 changes were 0.05 pmol kg^{-1}, 0.1 pmol kg^{-1} and 0.2 pmol kg^{-1} for 1997, 2003 and 2012, respectively. The CFC spreading between the DWBC and the Caribbean, from 1997 to 2012, matches the 10 year period of CFC expansion to the interior basin predicted by Joyce et al. (2001).

The DWBC flows eastwards north of Puerto Rico which is observed by two regions of high CFC at about 1500 m and 3500 m consisting of LSW and NOW, respectively (Figs. 7–8). The DWBC transports at this location varied in the 3 cruises. It was 41 Sv in 1997 (Joyce et al., 2001), 30.8 ± 10.3 Sv in 2003 and 17.7 ± 8.6 in 2012 (Table 2). The DWBC at the northern boundary of the section show high differences between the 1997 (−37.5 Sv, Joyce et al. (2001)) and 2003 (−17.3 ± 2.9 Sv) cruises. In contrast, the DWBC in 2003 and 2012 has a marginal difference not significantly different from zero (−14.9 ± 2.5 Sv in 2012). The northern DWBC fluxes are similar to those of Ganachaud (2003) at 48°N (−16 ± 2 Sv) and Macdonald (1998) at 36°N (−14 ± 5 Sv). The reduction of the DWBC fluxes between 1997 and 2003, at both paths, is probably due to the range of latitudes used to estimate the transport. The increment of ~13 Sv in 2003 between the northern and southern routes of the DWBC is possibly due to the entrainment of some water masses along its path from the north to the south. Toole et al. (2017) reported a statistically significant reduction of the DWBC between 2004 and 2014 (from −33.0 Sv to −25.9 Sv) that qualitatively agrees with our transport decrease between 2003 and 2012. It is worth mentioning that our results may have very strong aliasing due to the fact that our sections are separated about 10 years with a possible presence of seasonal transport variability and large geophysical noise (i.e., the CCR in the southern edge of the GS in 2012).

The GS transport varies seasonally being higher in winter/spring than in summer/fall (Sato and Rossby, 1995). For this reason, our results show an increase of ~20 Sv from 2003 (fall) to 2012 (spring) (100.1 ± 4.6 Sv in 2003 and 123.8 ± 4.6 Sv in 2012). In 1997, the GS carried 153–158 Sv, about 50 Sv more than in 2003. The larger 1997 transport is due to the different location of the 1997 occupation, such that NRG water entrainment by the GS is occurring, as pointed out by Hogg (1992). The position of the GS is also different between cruises, being more northerly in 1997 and 2012 than in 2003 (Fig. 16a). This is opposite to seasonal behavior described for the GS, which shows northward shifts of the GS in fall (2003), with a northernmost position in September and southward shifts in spring (2012) (Lee and Cornillon, 1995; Lillibridge and Mariano, 2013; Rayner et al., 2011). In contrast, the 2003–2012 shift of the GS matches with the changes in position of the GS described in Pérez-Hernández & Joyce (2014) from two decades of altimetry data, where 2012 is one of the three years with the northernmost position on the time series.

The 2012 recirculation of the GS is approximately 15 Sv lower than in 2003 (−43.0 ± 10.9 Sv and −59.8 ± 8.8 Sv, respectively, Table 2). The variation is probably produced by the CCR found at the boundary recirculation in 2012. Joyce et al. (2001) do not give any estimation of the GS recirculation in 1997 as its southern edge was unclear.

The heat fluxes over the three cruises are not significantly different (ranging between −0.21 and −0.25 PW) losing heat to the atmosphere. In contrast, freshwater fluxes showed what seems a marked seasonality. Freshwater fluxes in the area are observed to be positive in summer and spring (0.31–0.37 Sv in 1997 and 0.24 Sv in 2012) when the evaporation rates are higher than the precipitation rates, and negative in fall (−0.32 Sv), when the precipitation dominates over evaporation.

Acknowledgements

This study has been performed as part of projects: US CLIVAR Repeat Hydrography Program, which is now part of the International GO-SHIP project funded by the National Science Foundation, and BOUNDARY (ProID2017010083) funded by RIS-3, PO Feder Canarias. The wind data were collected from NCEP Reanalysis Derived data (http://www.esrl.noaa.gov/psd/). Hydrographic data were collected from the CCHDO website (https://cchdo.ucsd.edu/). The LADCP data were collected from Clivar/CO2 Repeat Hydrography Shipboard ADCP data program (http://currents.soest.hawaii.edu/clivar/ladcp). This work has been completed as part of MC-C work at IOCAG, in the doctoral program in Oceanography and Global Change. The first author would like to thank the Agencia Canaria the Investigación, Innovación y Sociedad de la Información (ACCISI) grant program of apoyo al personal investigador en formación, as well as to Woods Hole Oceanographic Institution (WHOI) for accepting as guest student to develop this study. The authors are also grateful to Rayco Alvarado and David Sosa for their help with figures and data analysis.

References

Bryden, H.L., Johns, W.E., Saunders, P.M., 2005. Deep western boundary current east of Abaco: mean structure and transport. J. Mar. Res. 63, 35–57. https://doi.org/10.1357/0022240053693806.

Centurioni, L.R., Niiler, P.P., 2003. On the surface currents of the Caribbean Sea. Geophys. Res. Lett. 30, 10–13. https://doi.org/10.1029/2002GL016231.

Chérubin, L.M., Richardson, P.L., 2007. Caribbean current variability and the influence of the Amazon and Orinoco freshwater plumes. Deep Res. Part I 54, 1451–1473. https://doi.org/10.1016/j.dsr.2007.04.021.

Comas-Rodríguez, I., Hernández-Guerra, A., McDonagh, E.L., 2010. Referencing geostrophic velocities using ADCP data Referencing geostrophic velocities using ADCP data. Sci. Mar. 74, 331–338. https://doi.org/10.3989/scimar.2010.74n2331.

Fisher, A., 1972. Entrainment of shelf water by the Gulf Stream northeast of cape hatteras. J. Geophys. Res. 77, 3248–3255. https://doi.org/10.1029/JC077i018p03248.

Fratantoni, D.M., 2001. North Atlantic surface circulation during the 1990's observed with satellite-tracked drifters. J. Geophys. Res. Ocean. 106, 22067–22093. https://doi.org/10.1029/2000JC000730.

Fuglister, F., 1955. Alternative analyses of current surveys. Deep Sea Res. 2, 213–229. https://doi.org/10.1016/0146-6313(55)90026-5.

Ganachaud, A., 2003. Large-scale mass transports, water mass formation, and diffusivities estimated from World Ocean Circulation Experiment (WOCE) hydrographic data. J. Geophys. Res. 108, 3213. https://doi.org/10.1029/2002JC001565.

Ganachaud, A., Wunsch, C., 2000. Improved estimates of global ocean circulation, heat transport and mixing from hydrographic data. Nature 408, 453–457. https://doi.org/10.1038/35044048.

Gordon, A.L., 1967. Circulation of the Caribbean Sea. J. Geophys. Res. 72, 6207–6223. https://doi.org/10.1029/JZ072i024p06207.

Hall, M.M., Joyce, T.M., Pickart, R.S., Smethie, W.M., Torres, D.J., 2004. Zonal circulation across 52°W in the North Atlantic. J. Geophys. Res. Ocean. 109, 1–23. https://doi.org/10.1029/2003JC002103.

Hernández-Guerra, A., Fraile-Nuez, E., López-Laatzen, F., Martínez, A., Parrilla, G., Vélez-Blechí, P., 2005. Canary current and north equatorial current from an inverse box model. J. Geophys. Res. 110, 1–16. https://doi.org/10.1029/2005JC003032.

Hernández-Guerra, A., Joyce, T.M., 2000. Water masses and circulation in the surface layers of the Caribbean at 66°W. Geophys. Res. Lett. 27, 3497–3500. https://doi.org/10.1029/1999GL011230.

Hernández-Guerra, A., Joyce, T.M., Fraile-Nuez, E., Vélez-Belchí, P., 2010. Using Argo data to investigate the Meridional Overturning Circulation in the North Atlantic. Deep Sea Res. Part I Oceanogr. Res. Pap. 57, 29–36. https://doi.org/10.1016/j.dsr.2009.10.003.

Hernández-Guerra, A., Pelegrí, J.L., Fraile-Nuez, E., Benítez-Barrios, V., Emelianov, M., Pérez-Hernández, M.D., Vélez-Belchí, P., 2014. Meridional overturning transports at 7.5N and 24.5N in the Atlantic Ocean during 1992–93 and 2010–11. Prog. Oceanogr. 128, 98–114. https://doi.org/10.1016/j.pocean.2014.08.016.

Hernández-Guerra, A., Talley, L.D., 2016. Meridional overturning transports at 30° S in the Indian and pacific oceans in 2002–2003 and 2009. Prog. Oceanogr. 146, 89–120. https://doi.org/10.1016/j.pocean.2016.06.005.

Hogg, N.G., 1992. On the transport of the Gulf Stream between Cape Hatteras and the Grand Banks. Deep. Res. 39, 1231–1246. https://doi.org/10.1016/0198-0149(92)90066-3.

Johns, W., Beal, L.M., Baringer, M.O., Molina, J.R., Cunningham, S.A., Kanzow, T., Rayner, D., 2008. Variability of shallow and deep western boundary currents off the Bahamas during 2004–05: results from the 26°N RAPID–MOC Array. J. Phys. Oceanogr. 38, 605–623. https://doi.org/10.1175/2007JPO3791.1.

Johns, W.E., Townsend, T.L., Fratantoni, D.M., Wilson, W.D., 2002. On the atlantic inflow to the caribbean sea. Deep Sea Res. Part I. Oceanogr. Res. Pap. 49, 211–243. https://doi.org/10.1016/S0967-0637(01)00041-3.

Joyce, T.M., Deser, C., Spall, M.A., 2000. The relation between decadal variability of subtropical mode water and the North Atlantic Oscillation. J. Clim. 13, 2550–2569. https://doi.org/10.1175/1520-0442(2000)013<2550:TRBDVO>2.0.CO;2.

Joyce, T.M., Hernandez-Guerra, A., Smethie, W.M., 2001. Zonal circulation in the NW Atlantic and Caribbean from a meridional World Ocean Circulation Experiment hydrographic section at 66°W. J. Geophys. Res. Ocean. 106, 22095–22113. https://doi.org/10.1029/2000JC000268.

Joyce, T.M., Pickart, R.S., Millard, R.C., 1999. Long-term hydrographic changes at 52 and 66° W in the North Atlantic Subtropical Gyre & Caribbean. Deep Res. Part II 46, 245–278.

Joyce, T.M., Thomas, L.N., Dewar, W.K., Girton, J.B., 2013. Eighteen degree water formation within the gulf stream during CLIMODE. Deep Res. Part II Top. Stud. Oceanogr. 91, 1–10. https://doi.org/10.1016/j.dsr2.2013.02.019.

Kalany, E., Kanamitsu, M., Kistler, R., Collins, W., Deaven, D., Gandin, L., Iredell, M.,

Saha, S., White, G., Woollen, J., Zhu, Y., Chelliah, M., Ebisuzaki, W., Higgins, W., Janowiak, J., Mo, K.C., Ropelewski, C., Wang, J., Leetmaa, A., Reynolds, R., Jenne, R., Joseph, D., 1996. The NCEP/NCAR 40-year reanalysis project. Bull. Am. Meteorol. Soc. 77, 437–471.

Kupferman, S.L., Garfield, N., 1977. Transport of low-salinity water at the slope water-gulf stream boundary. J. Geophys. Res. 82, 3481–3486. https://doi.org/10.1029/JC082i024p03481.

LeBel, D.A., Smethie, W.M., Rhein, M., Kieke, D., Fine, R.A., Bullister, J.L., Min, D.H., Roether, W., Weiss, R.F., Andrié, C., Smythe-Wright, D., Peter Jones, E., 2008. The formation rate of North Atlantic Deep Water and Eighteen Degree Water calculated from CFC-11 inventories observed during WOCE. Deep Res. Part I Oceanogr. Res. Pap. 55, 891–910. https://doi.org/10.1016/j.dsr.2008.03.009.

Lee, T., Cornillon, P., 1995. Temporal variation of meandering intensity and domain-wide lateral oscillations of the Gulf Stream. J. Geophys. Res. 100, 13603–13613. https://doi.org/10.1029/95JC01219.

Lillibridge III, J.L., Hitchcock, G., Rossby, T., Lessard, E., Mork, M., Golmen, L., 1990. Entrainment and mixing of shelf/slope waters in the near-surface Gulf Stream. J. Geophys. Res. 95, 13065–13087. https://doi.org/10.1029/JC095iC08p13065.

Lillibridge, J.L., Mariano, A.J., 2013. A statistical analysis of Gulf Stream variability from 18+ years of altimetry data. Deep Res. Part II Top. Stud. Oceanogr. 85, 127–146. https://doi.org/10.1016/j.dsr2.2012.07.034.

Macdonald, A.M., 1998. The global ocean circulation: A hydrographic estimate and regional analysis. Prog. Oceanogr. 41, 281–382. https://doi.org/10.1016/S0079-6611(98)00020-2.

Metcalf, W.G., 1976. Caribbean-atlantic water wxhange through the anegada-jungfern passage. J. Geophys. Res. 81, 6401–6409.

Pérez-Hernández, M.D., Joyce, T.M., 2014. Two modes of Gulf Stream variability revealed in the last two decades of satellite altimeter data. J. Phys. Oceanogr. 44, 149–163. https://doi.org/10.1175/JPO-D-13-0136.1.

Rayner, D., Hirschi, J.J.-M., Kanzow, T., Johns, W.E., Wright, P.G., Frajka-Williams, E., Bryden, H.L., Meinen, C.S., Baringer, M.O., Marotzke, J., Beal, L.M., Cunningham, S.A., 2011. Monitoring the atlantic meridional overturning circulation. Deep Sea Res. Part II Top. Stud. Oceanogr. 58, 1744–1753. https://doi.org/10.1016/j.dsr2.2010.10.056.

Sato, O.T., Rossby, T., 1995. Seasonal and low frequency variations in dynamic height anomaly and transport of the Gulf Stream. Deep Res. Part I 42, 149–164. https://doi.org/10.1016/0967-0637(94)00034-P.

Schmitz, W.J., McCartney, M.S., 1993. On the North Atlantic circulation. Rev. Geophys. 31, 29–49. https://doi.org/10.1029/92RG02583.

Schmitz, W.J., Richardson, P.L., 1991. On the sources of the Florida Current. Deep Sea Res. 38, S379–S409. https://doi.org/10.1016/S0198-0149(12)80018-5.

Smethie, W.M.J., 1993. Tracing the thermohaline circulation in the western North Atlantic using chlorofluorocarbons. Progre 31, 51–99.

Smethie, W.M.J., Fine, R.A., Putzka, A., Jones, E.P., 2000. Tracing the flow of North Atlantic Deep Water using chlorofluorocarbons. J. Geophys. Res. 105, 14297–14323.

Sou, T., Holloway, G., Eby, M., 1996. Effects of topographic stress on Caribbean Sea circulation. J. Geophys. Res. 101, 16449-. https://doi.org/10.1029/96JC00666.

Steinfeldt, R., Rhein, M., Walter, M., 2007. NADW transformation at the western boundary between 66°W/20°N and 60°W/10°N. Deep Res. Part I Oceanogr. Res. Pap. 54, 835–855. https://doi.org/10.1016/j.dsr.2007.03.004.

Stommel, H., 1965. The Gulf Stream: a physical and dynamical description. In: University of California Press (Ed.). Berkely, p. 248.

Stramma, L., Kieke, D., Rhein, M., Schott, F., Yashayaev, I., Koltermann, K.P., 2004. Deep water changes at the western boundary of the subpolar North Atlantic during 1996 to 2001. Deep Sea Res. Part I Oceanogr. Res. Pap. 51, 1033–1056. https://doi.org/10.1016/j.dsr.2004.04.001.

Talley, L.D., 2008. Freshwater transport estimates and the global overturning circulation: Shallow, deep and throughflow components. Prog. Oceanogr. 78, 257–303. https://doi.org/10.1016/j.pocean.2008.05.001.

Talley, L.D., Feely, R.A., Sloyan, B.M., Wanninkhof, R., Baringer, M.O., Bullister, J.L., Carlson, C.A., Doney, S.C., Fine, R.A., Firing, E., Gruber, N., Hansell, D.A., Ishii, M., Johnson, G.C., Katsumata, K., Key, R.M., Kramp, M., Langdon, C., Macdonald, A.M., Mathis, J.T., McDonagh, E.L., Mecking, S., Millero, F.J., Mordy, C.W., Nakano, T., Sabine, C.L., Smethie, W.M., Swift, J.H., Tanhua, T., Thurnherr, A.M., Warner, M.J., Zhang, J.-Z., 2016. Changes in ocean heat, carbon content, and ventilation: a review of the first decade of GO-SHIP global repeat hydrography. Ann. Rev. Mar. Sci. 8, 185–215. https://doi.org/10.1146/annurev-marine-052915-100829.

Toole, J.M., Andres, M., Le Bras, I.A., Joyce, T.M., Mccartney, M.S., 2017. Moored observations of the Deep Western Boundary Current in the NW Atlantic:2004–2014. J. Geophical Res. Ocean. 122, 1–18. https://doi.org/10.1002/2017JC012984.

Van Aken, H.M., 2000. The hydrography of the mid-latitude northeast Atlantic Ocean: I: The deep water masses. Deep Sea Res. Part I: Oceanogr. Res. https://doi.org/10.1016/S0967-0637(99)00092-8.

Vélez-Belchí, P., Pérez-Hernández, M.D., Casanova-Masjoan, M., Cana, L., Hernández-Guerra, A., 2017. On the seasonal variability of the canary current and the atlantic meridional overturning circulation. J. Geophys. Res. Ocean. 122, 1–21. https://doi.org/10.1002/2017JC012774.

Worthington, L.V., 1959. The 18° water in the Sargasso Sea. Deep Sea Res. 5, 297–305. https://doi.org/10.1016/0146-6313(58)90026-1.

Wunsch, C., 1996. The ocean circulation inverse problem. J. Fluid Mech. 352, 374–378.

Wunsch, C., 1978. The North Atlantic general circulation west of 50°W determined by inverse methods. Rev. Geophys. Sp. Phys. 16, 583–620.